Formation and decay of hot nuclei in 475 MeV, 2 GeV proton- and 2 GeV ³He-induced reactions on Ag, Bi, Au, and U

X. Ledoux,[1] H. G. Bohlen,[2] J. Cugnon,[3] H. Fuchs,[2] J. Galin,[1,*] B. Gatty,[4] B. Gebauer,[2] D. Guerreau,[1] D. Hilscher,[2] D. Jacquet,[4] U. Jahnke,[2] M. Josset,[1] S. Leray,[5] B. Lott,[1] M. Morjean,[1] B. M. Quednau,[1] G. Röschert,[2] H. Rossner,[2] A. Péghaire,[1] L. Pienkowski,[5,6] R. H. Siemssen,[1,7] and C. Stéphan[4]

[1]*Grand Accélérateur National d'Ions Lourds (GANIL) IN2P3-CNRS, DSM-CEA, BP 5027, F-14076 Caen-cedex 5, France*
[2]*Hahn Meitner Institute, Glienicker Strasse 100, D-14109 Berlin, Germany*
[3]*Université de Liège B-400 Sart-Tilman, Liège 1, Belgium*
[4]*Institut de Physique Nucléaire, IPN Orsay, BP 1, F-91406 Orsay-cedex, France*
[5]*Laboratoire National SATURNE (LNS) IN2P3-CNRS, DSM-CEA, F-91191 Gif-sur-Yvette-cedex, France*
[6]*Heavy Ion Laboratory, Warsaw University, Banacha 4, 02-097 Warsaw, Poland*
[7]*Kernfysisch Versneller Instituut (KVI), Zernikelaan 25, 9747 AA Groningen, The Netherlands*
(Received 19 August 1997)

The formation and decay of hot nuclei generated in the interaction of light projectiles (475 MeV and 2 GeV protons and 2 GeV ³He) on a series of targets (¹⁰⁷Ag, ¹⁹⁷Au, ²⁰⁹Bi, and ²³⁸U) are studied with an apparatus combining the efficient detection of neutrons in 4π sr and an accurate characterization of light charged particles, intermediate-mass fragments (IMF's), and fission fragments. A two-step approach with an intranuclear cascade process for modeling the initial off-equilibrium phase of the collision followed by a classical step-by-step evaporation—including fission competition—is used to reproduce the data. It is inferred from the model, which is found to reproduce several data sensitive to heat, that nuclei with temperatures exceeding $T = 5$ MeV are produced for a sizable part of the events, thus giving the opportunity to study the behavior of hot nuclei free from strong collective excitations which generally accompany nucleus-nucleus collisions. Most of the observed features related to particle emission or more specifically to particle evaporation are rather well accounted for by the model calculation. The evaporationlike IMF emission is generally rather weak, and does not show any rapid onset at the highest excitation energies as would have been expected in a genuine thermal multifragmentation process. Binary fission of the U-like target is shown to be a fairly probable channel at most excitation energies. Some of the characteristics of the fission channel are satisfactorily reproduced, but not all. [S0556-2813(98)02605-3]

PACS number(s): 25.40.Sc, 25.55.−e, 24.10.−i, 25.85.Ge

I. INTRODUCTION

The thermal properties of hot nuclei have been studied for a long time on the basis of different theoretical models [1–12]. In particular the maximum temperature that a nucleus can sustain has been shown to be very sensitive to the nuclear equation of state [6,9,10]. In most models [2,3,10] the only nuclear degrees of freedom considered are mass, charge (isospin), and temperature. Collective excitations such as nuclear deformation, compression, and spin are neglected. When some of these are considered in addition to temperature [11,12] they are shown to strongly reduce the maximum temperature that a nucleus is able to bear while remaining a self-bound object. Also, it has been known for a long time that collective excitations influence the decay pattern of excited nuclei quite strongly, which is well documented in the case of rotating nuclei [13–15].

A meaningful investigation of the decay properties of hot nuclei would thus require a good knowledge of not only their initial temperature but also of their collective excitations. This is quite difficult in heavy-ion-induced reactions, when all these quantities are present and evolve strongly as a function of impact parameter as shown in dynamical calculations [16]. In order to circumvent these difficulties, investigations involving light projectiles such as protons and antiprotons accelerated in the GeV range are being done [17–21]. The underlying idea consists in keeping the collective excitations sufficiently small to be disregarded, leaving the thermal effect dominant [22–26]. There are two additional advantages in studying hot nuclei ''prepared'' from light projectiles rather than from heavy ones. It can be shown from intranuclear cascade (INC) calculations that the thermal equilibration time is much shorter with light particles [17,22]. This is of special importance when considering higher and higher excitation energies since the characteristic decay time by particle evaporation [12,27] becomes closer and closer to the equilibration time [28,29]. In principle, one should thus be able to investigate nuclei at higher temperatures, using light projectiles in place of heavy ones. Finally, from a practical viewpoint, it is much easier to deal with one single heated nucleus in one event rather than with the two—or even more—excited nuclei left after a nucleus-nucleus collision (these nuclei are the projectilelike and targetlike nuclei and, sometimes, the neck between these which may decouple as one or several additional hot pieces of nuclear matter). At moderate bombarding energies (20–100 MeV/nucleon) the sources of the secondary products resulting from the decay of the hot species are not easily distinguishable, making their

reliable characterization very difficult. The existence of a single hot nucleus after a light projectile interaction can thus be considered as a major advantage.

The light particle- (either proton or antiproton) nucleus interaction is generally modeled in two steps: the first one is an intranuclear cascade between the incident particle and the nucleons of the target nucleus and then, when thermal equilibrium is achieved, an evaporation process succeeds. In some cases a preequilibrium step is added in between the INC and the evaporation steps. More recently a quantum-molecular approach has been developed in order to treat the dynamics of the collision, combined with a statistical decay model [30].

So far and due to the inclusive character of most experiments [31–36,19,37], essentially data integrated over the impact parameter were considered. As a consequence, only average excitation energies were often inferred and not their whole distribution. It is one of the aims of the present experiment to obtain—as tentatively tried elsewhere [38]—more detailed experimental information and thus to be able to subject model calculations to more stringent tests. Two different kinds of information are obtained. First, one can infer the initial excitation energy distribution and compare it with typical distributions obtained in nucleus-nucleus collisions. Then, one can compare their decay pattern with the one predicted by standard sequential decay models and explore whether for the hottest nuclei which are formed, ''new'' decay modes such as ''thermal multifragmentation'' occur. This is an important issue insofar as the comparison between nucleon-nucleus and nucleus-nucleus collisions is to be made. Indeed for the latter events there is so far no clear clue as to whether the so-called multifragmentation events are driven by thermal effects alone or whether they require in addition dynamical effects connected with collective modes. The study of hot nuclei ''prepared'' in an alternative way is thus expected to help to clarify this issue.

The neutron multiplicity measured on an event-by-event basis was chosen as the observable for excitation energy. Indeed it has been shown that evaporated neutrons are emitted in nearly any collision from a heavy nucleus in contrast to charged particles which require sufficient initial excitation energy in order to be released [39]. It was also shown elsewhere [40] that a neutron multiplicity meter is a very powerful and sensitive tool, well adapted to the study of hot nuclei, even if its sensitivity declines at high excitation energy when charged particles contribute substantially to the cooling down of the nucleus.

In addition to the neutrons, charged particles were also measured as their multiplicities provide additional constraints for the comparison with model calculations. Moreover, from their energy spectra, it was expected that ''spectral temperatures'' could be obtained as a function of neutron multiplicity. The detection of nuclei with masses intermediate between those of alpha particles and fission fragments—often referred to as intermediate-mass fragments (IMF's)—is also of great interest since a rapid increase of their abundance as a function of neutron multiplicity may reveal the onset of the so-called multifragmentation phenomenon.

When dealing with heavy target nuclei, fission is a widely open channel. The fission probability being very sensitive to the deposited excitation energy, spin, and characteristics of
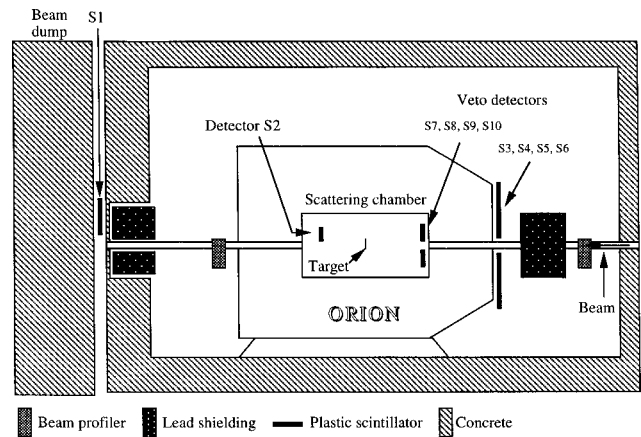
FIG. 1. Layout of the experimental setup at SATURNE in a side view. The scheme is not to scale.

the fissioning nucleus through the fissility parameter, fission is also a very interesting probe of the two-step process, i.e., nonequilibrium followed by an equilibrated system. A careful measure of fission with a precise determination of the angle between the coincident fragments thus allows a confrontation with modeled data.

It must be stressed that unlike most light-projectile–nucleus studies carried out so far, all described measurements were performed in coincidence with the neutron multiplicity used as the leading observable of the deposited energy.

The paper is organized as follows. In Sec. II, after a description of the experimental setup and of its properties, a detailed account will be given of the inclusive neutron multiplicity distributions on different targets with different projectiles. Then, in Sec. III, attention will be paid to charged particles measured in coincidence with the neutrons; their behavior will be shown to support the conclusions derived from the analysis of the neutron multiplicity data. Finally, fission will be considered within the same framework and difficulties encountered in the process aiming at reproducing all fission observables will be discussed. In Sec. VI, a summary and outlooks will be given.

II. EXPERIMENTAL SETUP AND MEASURED PARAMETERS

The experiment was performed with the proton and ^{3}He beams delivered by the synchrotron of the SATURNE national facility in Saclay. The detection system was installed on the SPES-IV spectrometer beam line, the spectrometer being used to transport the incident beam onto the target (either ^{107}Ag, ^{197}Au, ^{209}Bi, or ^{238}U) rather than a reaction product analyzer. Different types of detectors were set up to measure light charged particles (and IMF's) and fission fragments, respectively, with the neutron detector tank enclosing all these detectors (Figs. 1 and 2). The neutron detector ORION [41] is a 4π-sr detector of large efficiency. The charged particle detectors, housed in the 1-cm-thick scattering chamber of ORION made of stainless steel, consisted of ten silicon telescopes, located nearly in the same plane and spanning various directions relative to the beam. The fission detectors comprised two bidimensional position-sensitive,

ORION

experimental setup inside ORION
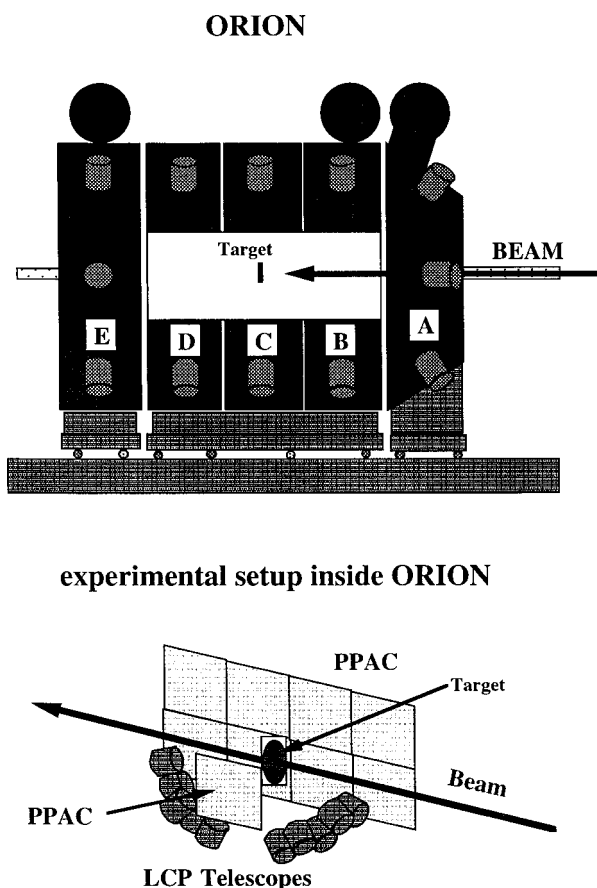
FIG. 2. Detailed sketch of the ORION neutron detector and associated charged particle and fission fragment detectors. ORION is 2.5 m long and 1.6 m in diameter. The size of the other detectors is given in the text.

low-pressure multiwire chambers [42]—named for simplicity parallel plate avalanche detectors in this paper—located roughly at 180° from each other and 90° to the beam direction.

Ten plastic scintillator detectors were also used, as sketched in Fig. 1, for tagging, vetoing, and monitoring the beam. In addition, a 2-mm-thick start detector (not shown on the lay-out), located about 30 m upstream from the target in the beam was used to get both a trigger and a time reference when taking inclusive neutron multiplicity data. It could not be used for the exclusive neutron measurements (here defined as measurements triggered by the detection of either light charged particles or fission fragments) due to the higher beam intensity then needed for these experiments. Detector S2 (2 mm thick) could be temporarily inserted in the beam for checking the transmission of the beam. This detector was removed during the data taking in order not to add background to the neutron data. A second detector, labeled S1, was set up close to the beam dump and outside the beam path—thus not generating background—in order to provide a permanent secondary monitor when counting particles generated in the beam dump. S1 (5 mm thick) provided a feedback signal necessary for the synchrotron to deliver a most steady intensity of particles within the spill. Additional large-area plastic scintillator detectors 630×370 mm^2 for S3–S6 and 100×100 mm^2, total area, for S7–S10 with an inner hole of 2 cm in diameter were used for vetoing the particles

(essentially charged particles or γ rays) present in a beam halo of primary or secondary particles which might have interacted with any material extending outside the target foil. Most of the beam was contained within a 1 cm^2 spot on target. The solid angle covered by S7–S10 is too small (about 1% of 4π) to veto legitimate events in a significant way. As will be shown later on, all these veto detectors were not 100% efficient; in particular they were much too thin (from 2 to 5 mm thick for S7–S10 and S3–S6, respectively) to register incident neutrons which could be parasitically generated upstream from the detection setup.

The 4π neutron detector is made of 4 m^3 of liquid scintillator (NE343 from Nuclear Enterprise). The tank, centered on the beam axis, with a total length of 2.5 m, houses a cylindrical scattering chamber (1.2 m long and 0.6 m in diameter) as sketched in Fig. 2. It is split into five optically separated sectors and the light readout was performed both globally and in each individual sector by means of six 5-in. phototubes (XP2041 from Philips) per sector. The scintillator is gadolinium loaded (0.3% in weight), allowing this detector to provide two types of information separated in time [41,43]. The first one is the prompt signal from the incident neutrons but equally from charged particles and γ rays, and the second results from the radiative capture of the thermalized neutrons, delayed by a few μs. The counting of the individual delayed signals provides the numbering of the captured neutrons. The detection efficiency was checked to be close to 80% for the 2 MeV neutrons of a ^{252}Cf source. In the present experiment both responses of ORION were exploited, the first providing a timing signal and, the second, the event-by-event neutron multiplicity. The high sensitivity of this very massive detector makes it also very susceptible to any kind of background. This turned out to be a major difficulty of the present experiment. It required a strong effort to shield the detector (with both concrete and lead) and to set up large-area veto detectors (S3–S10).

The neutron detector was operated in two different modes depending on whether the neutrons were recorded without any other requirement (which we will refer to as the ''inclusive measurements'') or they were recorded in coincidence with either charged particles or two fission fragments (to be labeled ''exclusive measurements''). The two operating modes were dictated by experimental constraints. In normal operation and without any beam, the neutron detector triggers with a rate of about 10^4 s^{-1} arising from the dark current of the phototubes and the natural background (e.g., γ decay from K contained in the concrete shielding and cosmic radiation). As a consequence such a detector cannot be triggered by itself but requires an independent external signal. In the inclusive mode the measurement was performed with a rather thick target (about 1 g/cm^2) at low beam intensity (typically 10^3 particles/s) whereas in the exclusive mode the target was much thinner (about 1 mg/cm^2) and the beam more intense (exceeding 10^6 particles/s) which made its tagging no longer possible. In the inclusive measurements, the rather thick target did not impair the detection of neutral particles and the low beam intensity minimized the background generated by the beam itself, thus optimizing the quality of the data. Conversely, very thin targets were required when detecting fission fragments and a high flux of impinging particles was then needed to assure reasonable

TABLE I. Main characteristics of the Si detector telescopes.

Detection angle (deg)	Detector thicknesses (μm)	Area (mm^2)	Distance to target (mm)
15	23.8, 296, 5000	300	125
30	12.6, 87, 500, 5000	300	125
45	25, 298, 5000	300	125
60	12.3, 70, 500, 5000	300	125
75	25, 301, 5000	300	125
105	12, 80, 500, 5000	300	125
120	26.5, 318, 5000	300	125
135	12.5, 95, 500, 5000	300	125
150	25, 315, 5000	300	125
165	12, 85, 500, 5000	300	125

statistics. The relative beam intensity was then monitored by the count rates in the telescopes rather than by the direct beam intensity measurements. After the coincidence requirement of at least two simultaneously fired phototubes (in order to minimize triggering on intrinsic phototube noise) coincident with either an incident particle or a charged particle or fission product had been fulfilled, a gate was opened 700 ns later for a duration of 70 μs. All light flashes occurring during the gate opening period were counted, thus providing the neutron multiplicity for each registered event. Corrections taking into account the background and the detector efficiency were performed when comparing the experimental data with model calculations and will be detailed later on.

The characteristics of the silicon diodes making up the telescopes, their positions and solid angles, are collected in Table I. Their combined solid angle amounts to 1.5% of 4π. The analog channels associated with each detector were twofold (with a low-high gain amplification) in order to extend the measured range in energy. Moreover, in order to minimize the capacitance of the 12-μm thick and 3 cm^2 detectors, the gold surfaces were divided in two independent halves on the same Si wafer with each half connected with a low-high gain amplifier. Energy calibrations were performed using essentially the punch-through energies and it was checked that the events were properly located on the expected E-ΔE lines. A punch-through energy for $Z=1$ isotopes of about 30 MeV prevented us from getting complete energy spectra for these particles but did not impair their counting as $Z=1$ particles. For $Z>1$ products there was hardly any upper energy limitation in the spectra, except for $Z=2$ at the most forward detection angles.

Two parallel plate avalanche counters (PPAC's) set, face to face, on both sides of the beam, were used to detect coincident fission fragments (the target being rotated by 45° with respect to the beam) and to measure their folding angle. Their active areas were 61×61 mm^2 and 244×122 mm^2, with the large detector designed as an ensemble of 4×2 adjacent parts identical to the small one [42]. The detector openings were 23.5° in both Θ and Φ for the first one and 77° and 47° in Θ and Φ, respectively, for the second one. The central anodes provided both timing (Δt) and energy (ΔE) signals whereas the two surrounding conducting cathodes were striped in X and Y, respectively, providing the position through a delay line readout with a resolution better than 1 mm. The ΔE and Δt signals allowed an unambiguous

identification of the fission events as exemplified in Fig. 3. Care was also taken of the consistency of the delay line readouts in order to reject events connected with a double hit on any fission detector. The folding angle calibration was checked through cold fission events of U for which the two fragments are emitted back to back.

The fission measurements were done only with the U target (0.4 mg/cm^2). The excessive thickness of the other targets prohibited a clear distinction between fission fragments and lighter charged products. In the data analysis, care was taken of kinematical cuts due to the finite size of the sweeper detector (defined as the largest one, the smaller one being considered as a trigger detector) and corrections were made using Monte Carlo simulations. Such corrections are completely negligible for the Θ folding angle due to the wide opening of the sweeper detector as compared to that of the trigger detector. For Φ, corrections are negligible for $d\Phi$ correlations within a $\pm20°$ range, which include more than 95% of all events.

III. NEUTRON MULTIPLICITY DATA

For heavy, i.e., neutron-rich, nuclei, the neutron multiplicity provides very valuable information on essentially all reaction channels since, in contrast to charged particles, neutrons are evaporated at any excitation energy above the one-neutron threshold. Moreover, since the ORION detector is also sensitive to γ rays, the zero-neutron events can also be measured. The neutron multiplicity distribution thus provides an overall, gross picture of the energy dissipation as already shown elsewhere [17]. It has been used all along in this study as the principal observable for the energy dissipation. In the following, we first discuss the inclusive data.

Two measurements were performed under similar beam conditions, with and without the target foil, in order to subtract spurious events. For each measurement the time delay between the ORION detector (from the prompt signal) and the plastic detector tagging the incident particles was registered. The time resolution of about 3 ns, mainly determined by ORION, was sufficient to distinguish between three families of events for essentially all targets (solid lines in Fig. 4). In addition to the central peak, due to nuclear reactions in the target foil itself, one distinguishes additional peaks, due to spurious reactions induced both upstream and downstream from the target with the most intense peak due to upstream
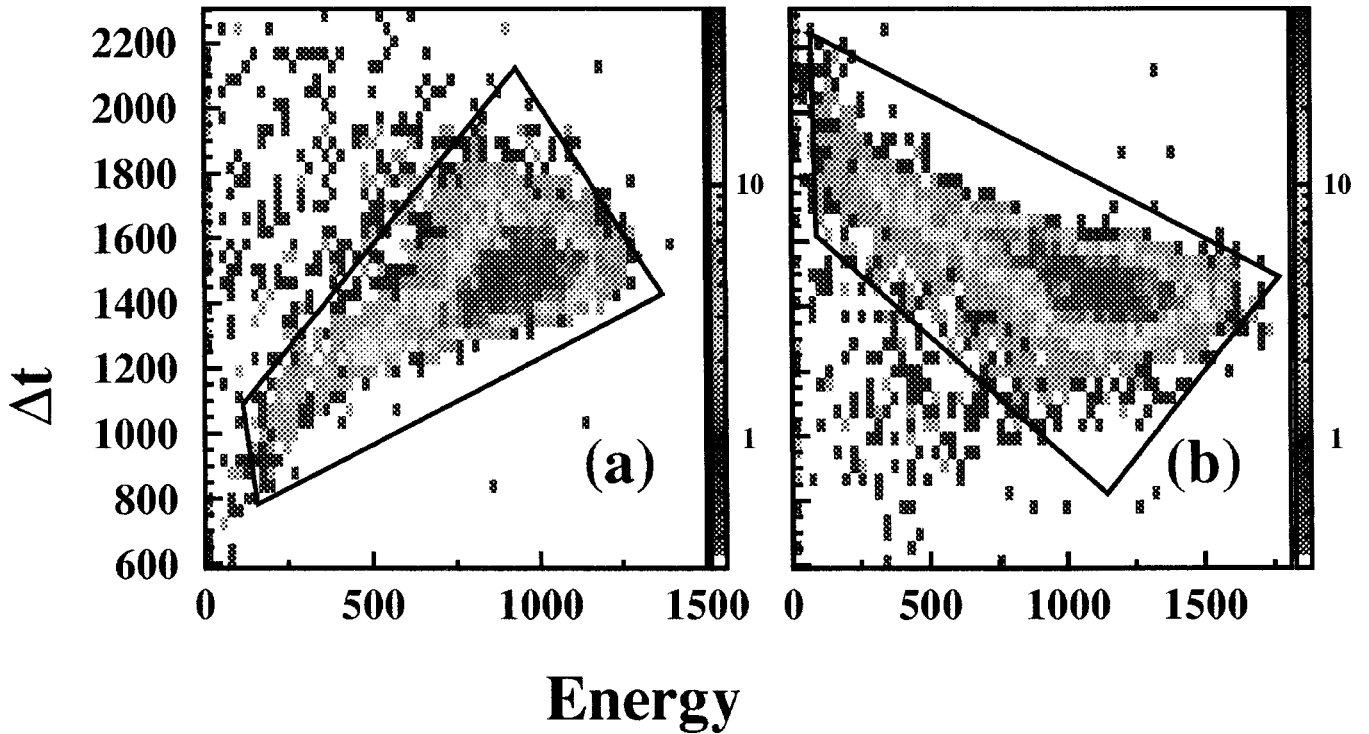
FIG. 3. Identification of the fission events by means of the energy versus relative time, both given in arbitrary units, for 2 GeV ^{3}He+U.

events. One can notice that the true events resulting from the thicker targets (784 mg/cm^2 Bi and 575 mg/cm^2 Au) are much more prominent than those obtained for thinner U and C targets (284 mg/cm^2 and 12.8 mg/cm^2, respectively). This justifies the choice of rather thick targets for the inclusive measurements. It must be emphasized that these targets are still thin enough to exclude secondary reactions within these targets. The measured times for the spurious events revealed that part of the incident beam (or spurious particles accompanying the beam and created by the beam itself in the SPES-IV spectrometer) hit the entrance of the ORION detector or the back wall of the scattering chamber housed inside ORION. This is confirmed by the relatively low multiplicity of the accompanying neutrons, as expected for low-Z materials such as iron, of which the containers are made, and the liquid organic scintillator. An application of the veto condition, generated by the large-area solid plastic scintillators S3–S10 located upstream from the neutron detector tank, was shown to reduce the intensity of spurious events for all three beams employed without modifying the intensity of target events (dashed lines in Fig. 4). Clearly the veto condition is not sufficient to fully clean up the data and one had to apply time gates in addition in order to select those events induced in the target. The same time gates were set for the data obtained in the absence of target foils but keeping the target environment the same (target frame and target frame holder).

Before subtracting the data obtained in the absence of a target, both types of data had been subjected to a correction of random background. The random background was measured in a continuous way by opening arbitrarily a second counting gate, delayed in time after any recorded event, of the same duration as the first counting gate.

The folded probability to measure n neutrons is given by

$$P1(n) = \sum_{m=0}^{n} P(n-m)P2(m),$$

where $P(n-m)$ and $P2(m)$ stand for the probabilities to have n true neutrons with m pseudoneutrons from the random background, respectively.

The unfolded probability $P(0)$ of measuring zero neutrons is thus given by

$$P(0) = P1(0)/P2(0),$$

where $P1(0)$ and $P2(0)$ stand for the measured probabilities of having zero neutrons in the first and second gates, respectively. More generally, the corrected probability for n neutrons is given by

$$P(n) = \left[P1(n) - \sum_{m=0}^{n-1} P(m)P2(n-m) \right] \Big/ P2(0).$$

A typical example of neutron multiplicity distributions as measured in the first and second gates (Fig. 5, top and middle, respectively) and the unfolded one (Fig. 5, bottom) is given for 2 GeV ^{3}He induced reactions on Au. The so-called background distribution exhibits two distinct parts: the low-multiplicity part which is essentially due to background from natural radioactivity and cosmic rays and the high-multiplicity plateau which arises from true random nuclear reactions on the target. The on-line comparison with the same part of the spectrum of Fig. 5 (top) allowed us to roughly estimate the amount of pileup and to tune the beam intensity accordingly. It can be seen that the correction on the mean neutron multiplicity amounts to 13% and that it affects essentially the low-multiplicity part of the distribution. Note also that the odd-even staggering which shows up
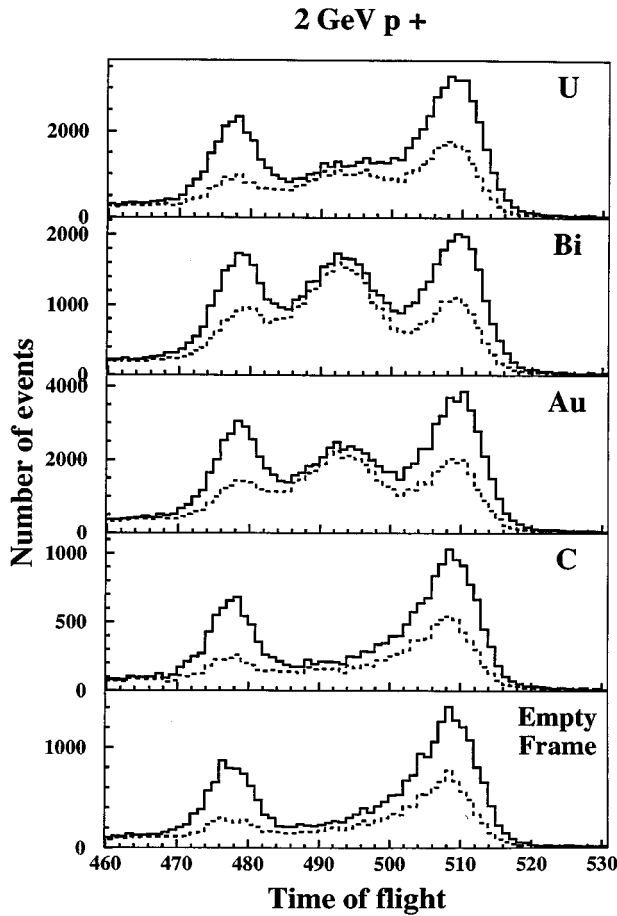
FIG. 4. Time spectra between the START detector and ORION as measured in 2 GeV *p*-induced reactions for U, Bi, Au, and C targets and an empty target frame. The solid and dashed lines represent measurements without and with the veto conditions as described in the text. The time runs from right to left and is given in arbitrary units.

FIG. 5. Measured neutron multiplicity distributions for the first-(top panel) and second- (middle panel) time gates and the result of background corrections (bottom panel), using the procedure described in the text. The considered reaction is 2 GeV ^{3}He+Au.

at high multiplicity in the final spectrum arises from the step-by-step unfolding procedure. Better statistics in the measured spectra would smooth them out.

As mentioned previously, the next step in the data reduction consisted in subtracting the distribution obtained in the absence of a target from those obtained with a target under the same beam conditions, i.e., normalized to the same number of impinging particles. Examples are given in Fig. 6 for the Bi target for the three different beams. The left-hand panels display the two above-mentioned multiplicity spectra and the right-hand ones their differences. The subtraction mostly affects the low-multiplicity part of the spectrum (up to three to four neutrons) and this clearly generates large uncertainties in the final values at this multiplicity level. However, it could be verified, when efficient tagging of the beam was achieved, which unfortunately was not always possible, that the total cross section derived from this neutron detection agrees satisfactorily with the geometrical cross section, as expected. This shows that with the described procedure the low-multiplicity events have been correctly recovered since in the absence of correction the total cross sections would be much in excess of the geometrical ones.

The final neutron multiplicity distributions for the ^{238}U,

^{197}Au, and ^{107}Ag targets obtained with the three projectiles are shown in Fig. 7. These are not corrected for the neutron detection efficiency that will be taken into account later in the comparison with the modeled data. It is also to be noted that the absolute cross sections have been determined by normalizing to the total reaction cross sections from independent sources. The starting point for this normalization is the $p+$Pb measurements [44] showing a small dependence of the reaction cross sections with the energy in the domain of interest. A cross section of 1600 mb is thus taken for this system from [44]. A simple $A^{2/3}$ geometrical scaling factor is then applied for the other targets the reaction cross sections of which have not been measured:

$$\sigma_{\text{geom}} = \pi(r_{\text{proj}} + r_0 A^{1/3})^2,$$

with $r_{\text{proton}} = 0.5$ fm, $r_{3\text{He}} = 1.5$ fm, and $r_0 = 1.15$ fm.

The thus obtained cross sections amount to 1969, 1763, and 1231 mb for proton-induced reactions and to 2338, 2108, and 1522 mb for the ^{3}He-induced reactions for U, Au, and Ag, respectively.

As was already shown in a previous publication of part of this experiment [17] the inclusive neutron data allow a critical test of model calculations and thus permit one to deduce to which degree a nucleus can be heated up in such light-particle-induced reactions. As usually done, two steps are considered in the reaction: a collision stage described by an intranuclear cascade process, followed by a standard cooling process setting in when thermal equilibrium has been achieved. In order to treat the first phase, the Cugnon model [22] was utilized and GEMINI [45] was used to model the decay of the heated nuclei. In comparison to other evaporation calculations such as PACE [46] the latter model has the

475 MeV p + Bi

2 GeV p + Bi

$d\sigma/dM_n$

2 GeV ³He + Bi

Neutron multiplicity
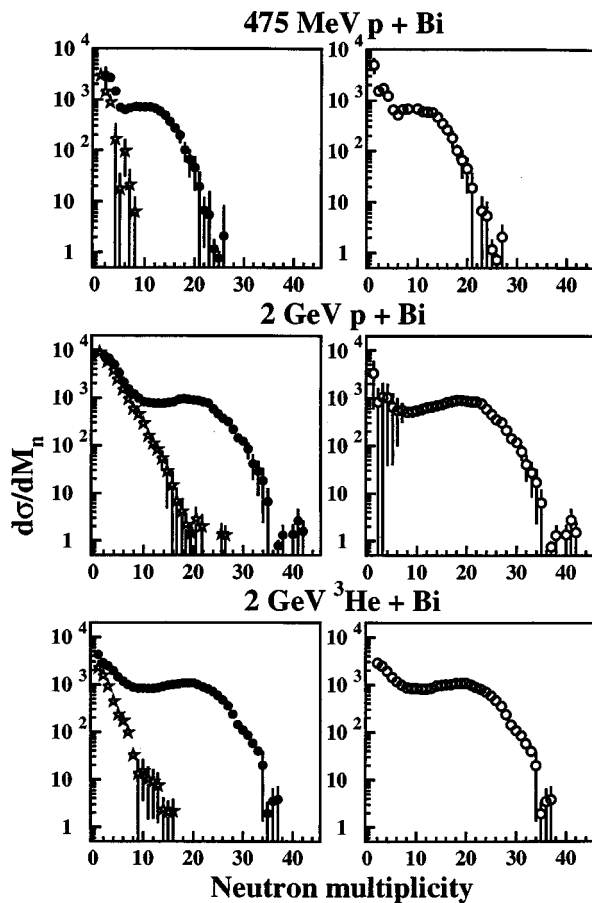
FIG. 6. Background-corrected neutron multiplicity distributions (in arbitrary units and not corrected for efficiency) with (solid dots) and without target (stars) and their difference (open dots) for p+Bi reactions at 475 MeV and 2 GeV (upper and middle panels, respectively) and for 2 GeV ³He+Bi (lower panels).

advantage of consistently treating intermediate-mass-fragment emission and fission, besides light particle evaporation. Fission barrier calculations were extended in the present use of the computer code to all nuclei of interest.

One of the difficulties of coupling the two reaction steps is the choice of the time at which one should switch from one step to the other. To plug in the evaporation code, thermal equilibrium should be achieved. We have thus investigated in detail various observables that may indicate the achievement of this thermal equilibrium in the first step. This is shown in Fig. 8 in which four different computed parameters are traced as a function of time. In the top panel are presented the cumulative number of nucleons having suffered at least one interaction with another particle—either hadron or meson (labeled ''participants'')—and the cumulative number of ejected nucleons (labeled ''ejectiles''). In the middle and bottom panels, the cumulative kinetic energy removed by the ejected particles and the excitation energy remaining in the nucleus are displayed, respectively. All quantities indicate an early fast evolution, before exhibiting a much smoother variation with time, indicative of some degree of equilibration. Consistently, the distribution of emitted particles evolves from a strongly forward emission pattern to a quite isotropic one. A sharp boundary cannot be inferred from the considered observables, but taking the equilibrium

as being achieved at $t=30\pm5$ fm/c looks reasonable. In Fig. 9 are shown the energy spectra of protons (right panels) and neutrons (left panels) from the INC calculation for the times $t<30$ fm/c (upper panels) and from the subsequent evaporation of the population of nuclei (defined by their A, Z, and excitation energy, their spin being neglected) formed by the INC (lower panels). Although the neutron spectra are much harder from the INC than from evaporation, they still exhibit a low-energy component which is not negligible when compared to the evaporative part. Making the assumption that the detected neutrons probe the thermal process alone is therefore too crude. This is confirmed in Fig. 10(a); even after folding the two neutron populations with ORION efficiency [47] the detected INC neutrons remain substantial (up to one-third of all detected neutrons) in spite of the low efficiency for high-energy neutrons. Summing up these two components on an event-by-event basis leads to the solid line in Fig. 10(b) that is to be compared to the data as they were measured (solid dots). The agreement is satisfactory and probably actually better than suggested by Fig. 10. Indeed, another correction should be applied before a fully meaningful comparison is possible: the high-energy particles emitted forward in the first steps of the INC may undergo secondary reactions in all the encountered materials (tank, scintillator, shielding, wall of the vault, etc.), resulting in extra neutron emission. Crude estimates with the CERN computer code GEANT [48] of the contamination amount to two to three neutrons depending on the input sets of parameters. Taking this component into account would further improve the agreement between the experimental and modeled data. However, because of the uncertainty associated with the secondary reactions, it is difficult to push the comparison between experiment and model much further. It can be shown that the results are quite insensitive to the time delay at which the evaporation process is chosen to set in: taking 25 fm/c or 35 fm/c instead of 30 fm/c does not modify the results significantly. Indeed, as noticed in a detailed inspection of the data globally shown in Fig. 9 for 30 fm/c, the particles emitted at the end of the INC stage or those considered at the beginning of the evaporation stage have pretty much the same characteristics (both in energy and emission angle) and can thus be described equally well by either model.

As shown in Fig. 7, there is the same overall satisfactory agreement between experimental data and model calculations for the two systems at 2 GeV. In the case of ³He projectiles, the INC calculation was run considering the three interacting nucleons with their Fermi momentum. It was found that the thermal energy distribution from 2 GeV ³He-induced reactions extends to slightly larger values than the one obtained from 2 GeV p on the same Au target. It was also checked for one system (2 GeV p+Au, Fig. 11) that the differential neutron multiplicity distributions, considering the five sectors of ORION (A–E as shown in Fig. 2), were in satisfactory agreement with the computed ones, thus indicating that the angular distribution of the neutrons is correctly reproduced as well. The rather poor agreement observed for the 475 MeV proton data in Fig. 7 is related to the rather poor quality of the beam at this energy. The excess of low-multiplicity events could not be completely removed by the procedure described previously.
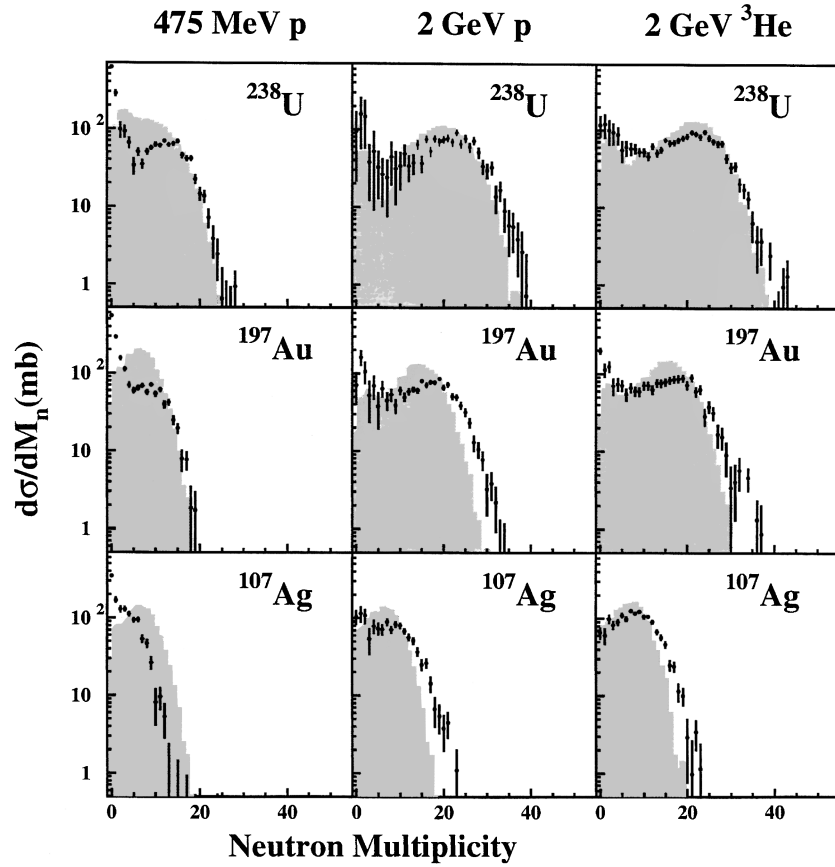
FIG. 7. Neutron multiplicity distributions as measured (without efficiency corrections) and after cross section normalization (for details see the text). The modeled data are depicted by the shaded areas.

Considering the neutron data to be in good agreement with the results of model calculations, the thermal energy distributions generated in the light-particle-induced reactions can be inferred by means of the model. This is shown in Fig. 12 considering a mean time of 30 fm/c for the achievement of thermal equilibrium as well as for 25 and 35 fm/c considered as reasonable lower and upper limits for this time. It is seen that, in contrast to previous estimates [22,49], the excitation energy distributions are not exponentially decreasing but instead are rather flat over a broad range and decreasing nearly exponentially only in the tail of the distributions. It is shown also that, whatever the chosen time, a sizable fraction of the nuclei are excited to high energies, this fraction being obviously larger for shorter thermalization times. It is shown in Fig. 13 how the computed excitation energy distributions depend on the nature and energy of the beam and on the nature of the target (Au and U). The excitation energies increase with the Z of the target for all projectiles and ^{3}He at 2 GeV is slightly more effective than 2 GeV protons in depositing its energy (this will be confirmed when considering the associated multiplicities of evaporationlike charged particles). These excitation energies are similar to the ones achieved in heavy-ion reactions induced at several tens of MeV/nucleon [39,50] and this makes the present approach competitive at least in so far as high temperatures are achieved. It should be recalled that the collective degrees of freedom are weakly excited in light-particle-induced reactions in contrast with heavy-ion-induced reactions. The excitation energies of 3–4 MeV/nucleon which are evidenced in
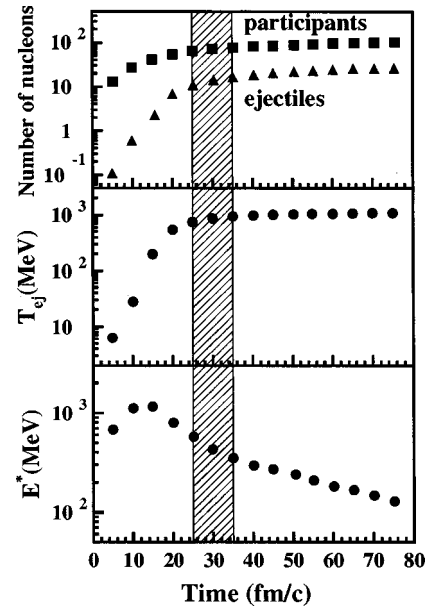
FIG. 8. Evolution as a function of time of four quantities computed using the INC as described in Ref. [15]. These are, from top to bottom, the cumulative number over time of nucleons having suffered one collision at least (solid squares), the cumulative number of ejected nucleons (solid triangles), the cumulative kinetic energy T_{ej}, removed by the ejected nucleons (middle panel), and the excitation energy left in the residual nucleus (bottom panel). A change of regime for all considered quantities is apparent for a time equal to 30 ± 5 fm/c.
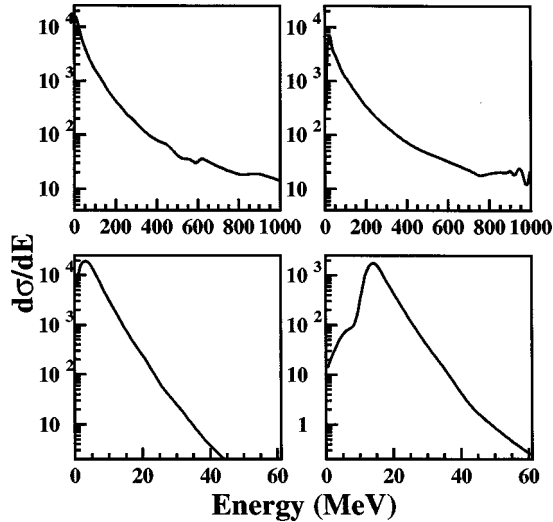
FIG. 9. Angle-integrated kinetic energy distributions (in arbitrary units) for the 2 GeV p+Au system computed with the INC model (upper panels) and with GEMINI (lower panels) for neutrons (left panels) and protons (right panels).

the tails of the distributions of Figs. 12 and 13 are to be taken as thermal energies in contrast to what is often quoted in heavy-ion studies as thermal excitation, being actually the sum of thermal and collective energy (expansion energy, flow energy).

To summarize, the neutron multiplicity data obtained with 2 GeV proton and ^{3}He projectiles show that high thermal energies can be generated in a nucleus with sizable cross sections and that a two-step model can fairly well account for these features.

IV. LIGHT CHARGED PARTICLE AND INTERMEDIATE-MASS FRAGMENT EMISSION

With the neutron multiplicity variable as a sensitive observable of the excitation energy, the study can be pushed further by investigating the behavior of light charged particles and intermediate-mass fragments measured in coincidence with the neutrons. Because of the experimental conditions, the information on $Z=1$ and $Z>3$ is limited to their multiplicities. For $Z=1$, the telescopes were not thick enough to get complete energy spectra, and for $Z>3$, the statistics was too poor to obtain meaningful energy spectra.

The inclusive energy spectra measured at 15°, 30°, 60°, 120°, 135°, 150°, and 165° are shown in Fig. 14 for $Z=2$ particles produced in the p- and ^{3}He-induced reactions at 2 GeV bombarding energy and for $Z=3$ nuclei obtained in the ^{3}He-induced reactions. They all exhibit a strong evolution with emission angle, with a more and more pronounced high-energy tail when moving from backward to forward angles. However, the maximum of the spectra remains essentially constant with angle, both in position and intensity. This low-energy part of the spectra is dominated by statistical evaporation from an emitter close to rest in the laboratory frame and this is also shown when considering the Galilean-invariant cross sections as a function of parallel and transverse velocities of these particles. Recoil velocities are
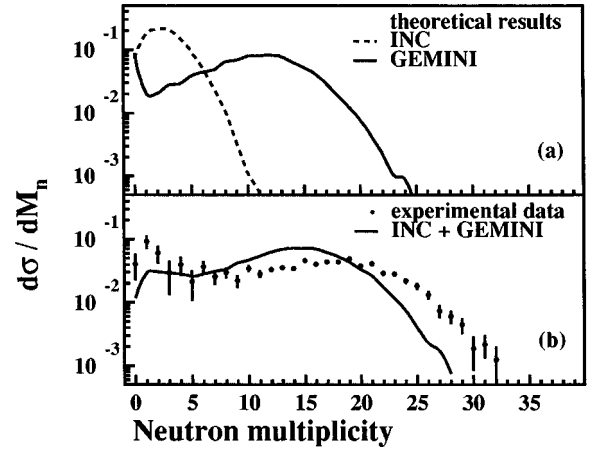
FIG. 10. (a) Neutron multiplicity distributions (in arbitrary units) as derived from the INC model (dashed line) and evaporation model (solid line) for the 2 GeV p+Au system after folding with the detector efficiency. (b) The event-by-event total multiplicity distribution (also folded by detection efficiency) is given by the solid line, to be compared with the measured data (solid dots). The matrix for neutron detection efficiency has been built as a function of emission angle and energy of the neutron, using the computer code DENIS [47].

roughly estimated to be 0.07 and 0.03 cm/ns for the ^{3}He- and proton-induced reactions, respectively, which corresponds to about one-tenth the initial projectile momentum. It has been tried to derive the recoil velocities for several gates in the neutron multiplicity, but due to the low statistics and the resulting large uncertainties, no clear evolution could be observed. It will be shown later on that fission fragments
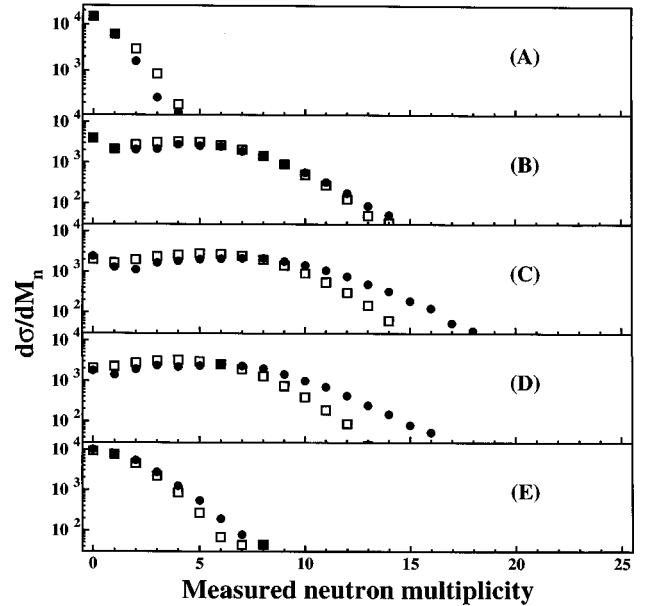
FIG. 11. Measured neutron multiplicity distributions (in arbitrary units) for the 2 GeV p+Au system with the five sectors of ORION (solid dots) and simulated ones (open squares) with the two-step model (filtered with the detector acceptance). The sectors are labeled A, B, C, D, and E from the most backward one, A, to the most forward one, E, as sketched in Fig. 2. The error bars are within the size of the data points.
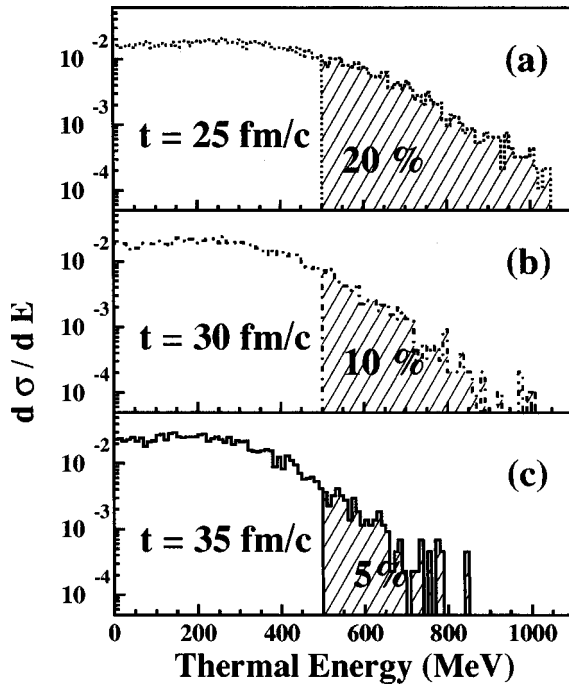
FIG. 12. Thermal energy distributions for the 2 GeV $p+$Au system (given in arbitrary units) computed with a thermalization time of 30 fm/c and lower and upper limits of 25 and 35 fm/c, respectively. The hatched areas represent the fraction of the cross section corresponding to thermal energies exceeding 500 MeV or temperatures $T>5$ MeV (considering the level density parameter $a=A/10$).

with a comparatively intrinsic lower velocity than ^{4}He are much more sensitive to the recoil. In the following data analysis the previously deduced recoil values have thus been retained, independent of the associated neutron multiplicities. The considered velocities are so low that the uncertainty
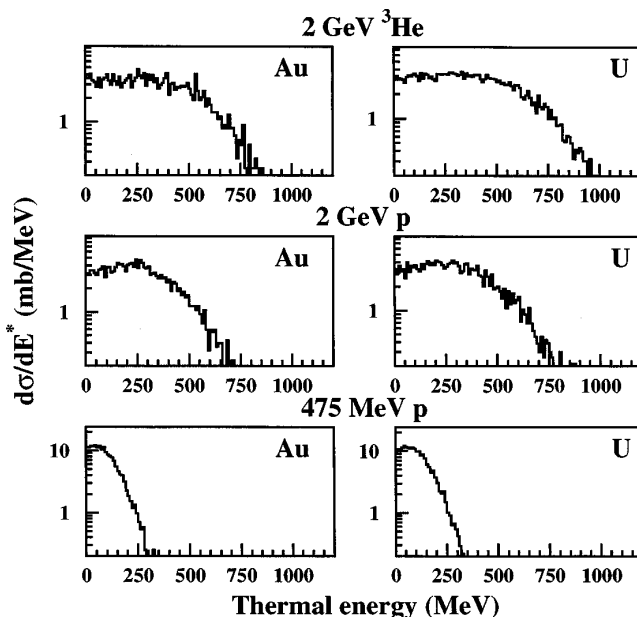
FIG. 13. Calculated thermal energy distribution cross sections (in mb/MeV) for the 2 GeV ^{3}He and 2 GeV and 475 MeV proton reactions on Au and U.
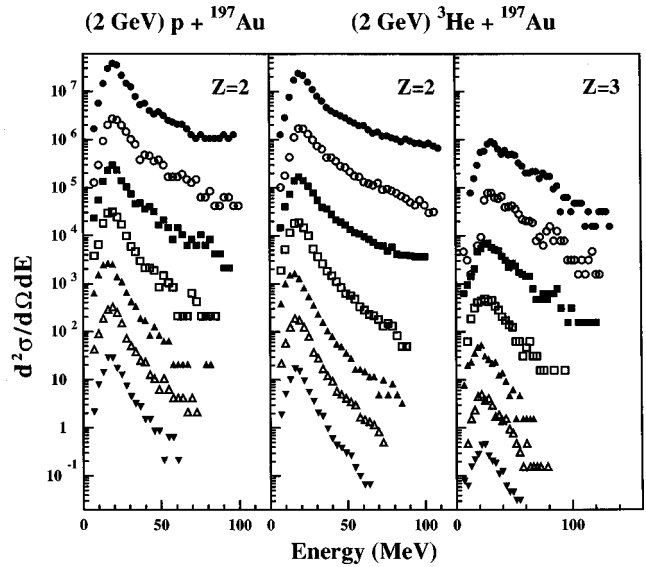
FIG. 14. Measured energy spectra at various angles from bottom to top: 165°, 150°, 135°, 120°, 60°, 30°, and 15° for alpha particles (in 2 GeV p- and ^{3}He-induced reactions on Au) and Li nuclei (in 2 GeV ^{3}He+Au). The ordinates given in arbitrary units are shifted by one order of magnitude for neighboring angles.

with which they are known has no influence on the transformation of the energy spectra when going from the laboratory reference frame to the emitter reference frame.

The energy spectra, whatever the detection angle, have two distinct components: the low-energy part, quite insensitive to the angle, which essentially arises from an evaporation process and, in contrast, the high-energy component, which varies in intensity with the emission angle and reflects the preequilibrium stage of the collision. It must be stressed that, although weak at backwards angles, it is still present, thus making it difficult to extract the temperatures from the slopes of the spectra, as we will show later. It can be noted that a reproduction of the high-energy tail is not possible within the adopted two-step model, INC+GEMINI, as the INC step considers nucleons and not clusters of nucleons. This is a deficiency of the present INC model that could be overcome by using quantum-molecular-dynamics treatments [51,52]. In the second step the nucleus is considered to be totally equilibrated and thus it is unable to generate an anisotropic high-energy component.

In the range of the measured angles (15°–165°) it is remarkable that the energy spectra for $Z=2$ look quite similar in shape at a given angle, irrespective of the type of projectile, a 2 GeV p or a 2 GeV ^{3}He (Fig. 14). More amazing are the observed similarities at all angles of the high-energy components. Why should the preequilibrium He emission be the same starting from proton or ^{3}He projectiles? No obvious answer could be found and a dedicated experimental program will be needed to understand this aspect. In particular, since it was shown [33,53] in the past that the emission of ^{3}He and ^{4}He probes quite different instants of the reaction, a distinction of the two isotopes would be very useful to study this aspect. In our experiment the two isotopes were too poorly separated—especially at low energies—to obtain relevant information on this.

As mentioned above, attempts were made to study tem-
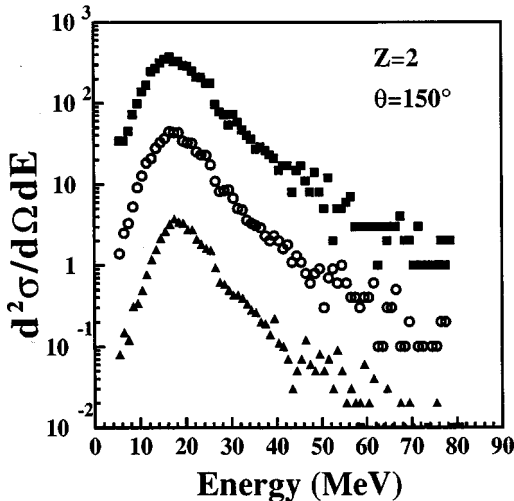
FIG. 15. Energy spectra of alpha particles detected at 150° in the 2 GeV ^{3}He+Au reaction, gated by three neutron multiplicity bins (25–34 measured neutrons, solid squares; 19–24 neutrons, open dots; and 10–19 neutrons, solid triangles). The ordinate scale is given in arbitrary units. Note that the discontinuity at 26 MeV corresponds to the punch-through of the 315-μm-thick Si diode of the telescope.

peratures from the energy spectra as a function of neutron multiplicity. Three gates were set in order to assure similar statistics. Corresponding spectra are shown in Fig. 15. In spite of the low statistics, it can be observed, even for backward emission, that the high-energy part of all three spectra cannot be fitted by a single exponentially decreasing function. Assuming an exponential falloff for the highest-energy tail of the spectra as also observed elsewhere for INC emission [54], the spectra were arbitrarily fitted with two Maxwell-Boltzmann distributions, with the only constraint of the same Coulomb barrier for the two distributions. The interesting result is the slope parameter of the low-energy distribution which provides an apparent temperature of the thermalized nuclei. As seen in Table II, within the experimental uncertainties, there is no clear evolution of the temperature as a function of the coincident neutron multiplicity. The absolute temperatures are relatively low as compared to what is inferred from the neutron multiplicity data. In such an analysis the slope provides an apparent temperature averaged over a long evaporation chain. A value lower than the initial temperature is thus expected. Moreover, the fitting procedure is rather crude with the high-energy contribution arbitrarily fitted by a Maxwell-Boltzmann distribution. Finally one can conclude that the choice of composite particles instead of

TABLE II. Spectral temperatures deduced from various neutron multiplicity gates for 2 GeV p+Au and 2 GeV ^{3}He+Au reactions. T_s and T_v stand for surface and volume emission, respectively.

Reaction	T (MeV)	Mn=10–19	Mn=20–24	Mn=25–34
^{3}He+Au	T_s	3.5± 0.3	3.6±0.3	3.9±0.3
p+Au	T_s	4.1±0.3	3.9±0.5	3.7±0.6
^{3}He+Au	T_v	4.2±0.3	4.6±0.5	4.8±0.4
p+Au	T_v	4.4±0.3	4.5±0.3	4.8±0.3

nucleons for inferring nuclear temperatures from the slopes of their energy spectra does not appear much better than what could be done with noncomposite particles, more susceptible to direct emission in the first step of the reaction. Fortunately, the intensity of the nonequilibrium emission at backward angles is weak whatever the considered particle and does not preclude a precise determination of the intensity of the evaporative component. In the following, this intensity is exploited as a function of the neutron multiplicity.

As already mentioned, inclusive neutron multiplicity measurements and measurements of light charged particles together with the accompanying neutrons were done separately under quite different conditions of target thickness and beam intensity. The charged particle cross sections and multiplicities could not be obtained directly in the absence of knowledge of the beam flux during such measurements. The beam flux was obtained indirectly using a relative monitoring via the forward telescopes themselves. The proton loss by absorption inside the thick targets used in the inclusive measurements was carefully taken into account. Because of the rather low statistics of the measured protons in the monitor telescopes in the so-called inclusive measurements, the uncertainties in the charged particle multiplicities (this will be also true for the fission probability considered later) arise essentially from the uncertainties in the normalization factors and amount to about 10% and 20% for the He and proton experiments, respectively. The integration of the energy spectra over angle and energy is based on the backward angles (from 120° to 165°) where a quasi-isotropic angular distribution was found, as expected for evaporation in absence of spin. This was checked on $Z=2$ particles after subtraction of the high-energy component of the spectra. Actually the intensity of the nonevaporative part of the spectra is so low at backward angles that it can be considered to be negligible as far as cross sections are considered. The same procedure was used for particles with $Z=1$ and $Z>2$. The latter are strongly dominated by the lightest elements (Li, Be, B) and their yield drops off very rapidly with increasing Z. It was checked that the low-energy detection threshold does not affect the measured IMF energy spectra in a significant way. Thus the integrated multiplicities are practically unbiased. In Fig. 16 the angle-integrated multiplicities of the different types of evaporationlike particles are shown as a function of the associated neutron multiplicity. As anticipated for an evaporation process from a heavy nucleus [39], charged particle evaporation sets in only for large excitation energies, leading mostly to a large number of neutrons. It can also be seen that the emission of an IMF requires even more energy. The predictions of GEMINI when using as inputs the nuclei left by the INC process are given by lines in Fig. 16. Evaporation is shown to reproduce fairly well—i.e., essentially within the experimental absolute uncertainties quoted before—the general trend of the data especially for $Z=1,2$ particles. For the IMF's, the model underestimates the measured data with both projectiles. However, the average IMF multiplicity remains very small (smaller than 0.25) for the most dissipative collisions selected by the neutron multiplicity filter, corresponding to thermal energies larger than 500 MeV. These data can be compared with those measured for the same ^{3}He+Au system at 1.8 GeV [20,21]. In these papers, a similar IMF multiplicity evolution is shown as a func-
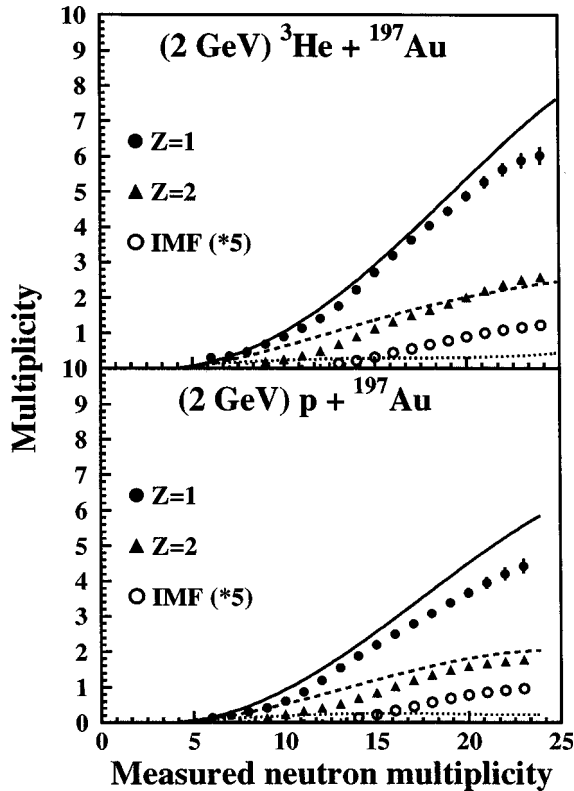
FIG. 16. Multiplicities of evaporated particles as measured for $Z=1$ (solid dots), $Z=2$ (triangles), and $Z>2$ (open dots and data multiplied by a factor of 5) as a function of neutron multiplicity (as measured without background correction). The lines are consistently derived from the two-step model and represent $Z=1$ (solid lines), $Z=2$ (dashed lines), and $Z>2$ (dotted lines after multiplication by a factor of 5). The given error bars of statistical origin do not include the absolute uncertainty due to normalization between inclusive and exclusive data. These amount to $\pm 10\%$ and 20% for the 2 GeV ^{3}He and p data, respectively.

tion of the multiplicity of charged particles: the maximum average multiplicity of $M_{IMF}=0.4$ instead of 0.25 in the present data is thought to stem from the way evaporationlike IMF's were selected. Considering the backward-emitted IMF's with further integration on 4π, as done here, is slightly more restrictive than a selection with an energy cut-off, as performed in Ref. [20]. If thermal multifragmentation is present at all—and this was not possible to probe directly in absence of a 4π measurement for charged particles—the probability for such a process appears to be fairly small even for the highest excitation energies which are reached in the present experiment. A similar observation has been made in antiproton-induced reactions with thermal energies up to 1000 MeV [18]. When compared with IMF multiplicities from nucleus-nucleus collisions [55] the present multiplicities are fairly small, thus giving an indication that the IMF emission in nucleus-nucleus collisions has little to do with a thermal process—as already pointed out elsewhere [56]—but that it is rather due to the dynamics of the collision. The recently observed [57,58] neck emission component with the neck between the projectilelike and the targetlike nuclei, which also contributes to an increased IMF multiplicity in heavy-ion-induced reactions, obviously cannot occur in proton-induced reactions. The difference in IMF multiplicity

may also stem from the fact that in nucleus-nucleus collisions the nuclei are left deformed, compressed, and spinning in contrast with the conditions that are achieved in a light-particle–nucleus collision.

Returning to the measured energy spectra of the IMF's in the present experiment it can be seen in Fig. 14 for $Z=3$ that their pattern evolves as a function of angle very similarly to that of lighter particles. At forward angles there is a high-energy tail which cannot be accounted for by an evaporation process. Such observations were first made long ago [35,54] on similar systems but have never received any satisfactory interpretation. In particular the INC model that we used has not considered the buildup and emission of complex particles from the interacting nucleons. Clearly, different theoretical approaches should be followed to account for off-equilibrium cluster emission [30,51,52].

V. FISSION

Fission has been measured for 475 MeV p+U and 2 GeV ^{3}He+U with sufficiently good statistics to be studied in detail together with the other measured observables. In particular, the measurement of fission as a function of the neutron multiplicity provides information on the fission process as a function of excitation energy which could not be obtained in previous light-particle-induced fission experiments [59–67]. In these experiments, fission was studied globally or, at best, as a function of one observable of the fission process itself, e.g., the folding angle of the fission fragments.

As shown in Fig. 3 the fission events were unambiguously identified using the ΔE signals in both PPAC's and their relative time of flight. This allowed us in particular to reject the few coincidence events between an IMF and a fission fragment. Figure 17 exhibits the $\Theta_1+\Theta_2$ folding angle distributions as a function of neutron multiplicity. With increasing violence of the collision the average folding angle of the fragments is seen to deviate more and more from 180°, becoming broader and broader. The first effect reflects the importance of the linear momentum transfer and the second one the increasing influence of particle evaporation prior to and subsequent to fission. The same series of plots has been generated from the two-step model as a function of neutron multiplicity. It should be recalled that the neutron multiplicities of the calculated data are folded with the neutron detector efficiency in order to get model data directly comparable to the face-to-face experimental data of Fig. 17. For 475 MeV p+U, a mean shift of the distribution of about 5° is observed on the average folding angle values independent of the dissipated energy. The overall distribution (summed over all neutron gates) has been checked against very similar experimental data (500 MeV p+Th) [63] and shown to agree very well, thus giving full confidence in the data. The model clearly fails and this is best seen for the less violent collisions (low neutron multiplicity) when no recoil is expected to be imparted to the fissioning nucleus and where the two fission fragments must be emitted back to back in the laboratory frame. It can be noticed that, in contrast, the second moments of the distributions are pretty well reproduced by the model. This is not contradictory with the failure in reproducing the first moments since the two observables are sensitive to different aspects of the process. The widths of the
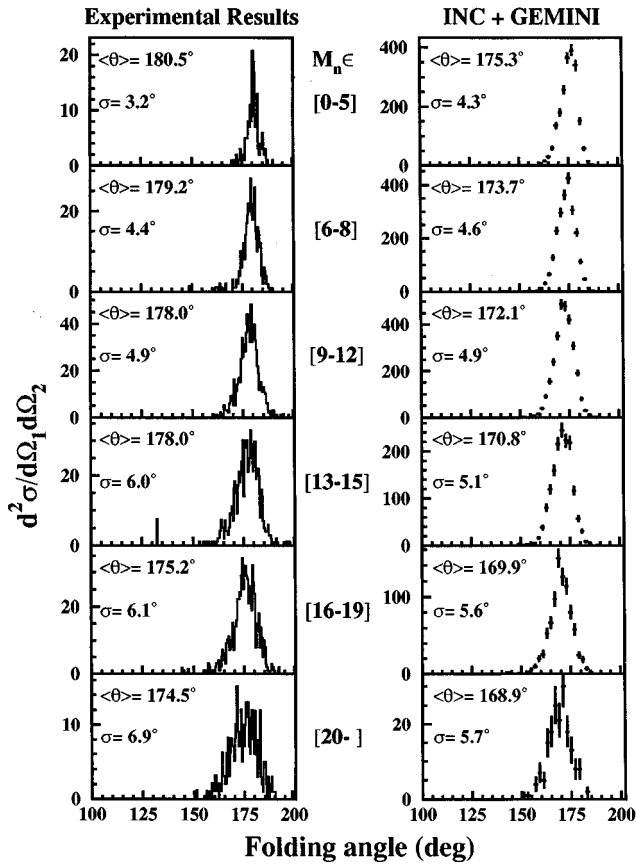
FIG. 17. Folding angle distributions of the fission fragments (as measured without background correction on left-hand panels and as computed on right-hand panels) as a function of the measured neutron multiplicity for 475 MeV p+U. The ordinate is given in arbitrary units.

FIG. 18. Same as for Fig. 17 for 2 GeV ^{3}He+U.

distribution are related to the first and second steps of the process, whereas the position of the centroids depends mostly on the first step of the collision. It is suspected that the failure to reproduce the momenta is related to computational problems (small differences of two large quantities). It should be stressed that excitation energy and momentum transfer are computed independently by the INC model that we used and this explains why the failure in the linear momentum estimate does not imply a failure in reproducing the excitation energy distribution. As shown before, the data sensitive to the latter parameter are fairly well reproduced.

The same analysis has been performed on fission following the ^{3}He+U reaction at 2 GeV (Fig. 18). Here again one observes a shift in the location of the maxima in the folding angle between the experimental and the simulated data. In contrast with the preceding discussion, this shift is not constant but increases with the heat initially deposited in the nucleus. Again, the model calculations are most likely at fault: an average $\Theta_1 + \Theta_2$ value of 146° as found for the most heated fissioning nuclei would correspond to a momentum transfer equaling 2/3 of the projectile momentum. This seems difficult to reconcile with excitation energies which were shown to never reach more than 40% of the total available energy. Once again the second momenta of the distribution are satisfactorily reproduced, indicating that the evaporation process preceding or following fission is fairly well

accounted for. However, this satisfactory agreement on the widths could be somewhat accidental if one remembers that nonequilibrium clusters are observed in the experimental data whereas they are not considered in the present model. Such off-equilibrium cluster emission is expected to broaden the distribution more than nucleons emitted sequentially and should thus translate into larger widths than those modeled. It is in contrast to the experimental data which are narrower than the calculated ones.

Another way to check the model was followed by studying the fission probability as a function of excitation energy. As was shown above the light particle evaporation is quite well reproduced by the model calculations, in particular the average multiplicities of the evaporated $Z=1,2$ particles as a function of the detected neutron multiplicity M_n. Can the same agreement be found for fission? The fission probabilities as a function of measured neutron multiplicity are shown in Figs. 19 and 20 for 475 MeV p+U and 2 GeV ^{3}He, respectively. The probabilities were obtained from the ratio of the number of fission events (after integration over 4π, assuming an isotropic distribution) to the total number of events associated with the same M_n value. For the ^{3}He experiment, the absolute normalization factor was obtained from the exclusive and inclusive measurements, as described before. For the 475 MeV proton experiment, this was not possible with sufficient accuracy and hence the normalization has been done arbitrarily, such that the fission probability saturates at 100% for a measured neutron multiplicity of 10. It is shown in Fig. 19 that the model calculations, performed without considering the spin generated in the first
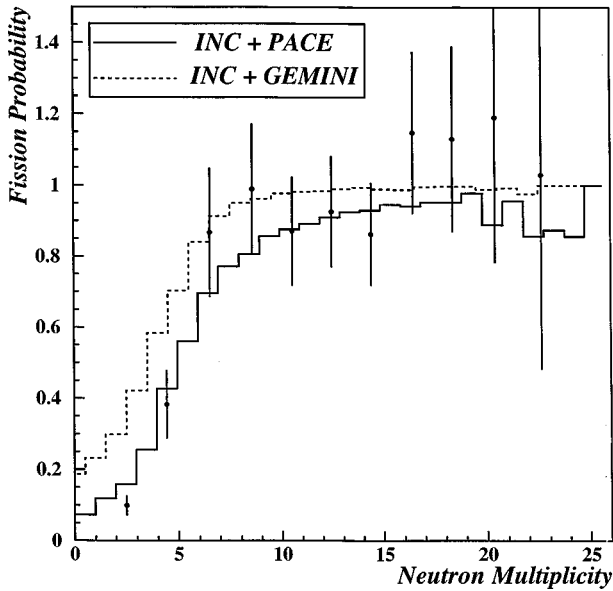
FIG. 19. Average fission probabilities for 475 MeV p+U as a function of measured neutron multiplicity without background correction (dots) and comparison with the two-step model, using INC +GEMINI (dotted line) and INC+PACE (solid line).

step, account for the experimental data pretty well over the whole range of excitation energies for the proton experiment. In particular at high excitation energies the fission probability is found to stay close to 100% which results essentially from the high fissility of the nuclei left at the end of the INC step. In contrast to the conclusions of Ref. [65], no hindrance of fission is observed at high excitation energy. The large number of prescission neutrons measured in Ref. [65] for the same system does not seem to affect the fission probability.

The situation is somewhat different for the 2 GeV ^{3}He-induced reactions (Fig. 20). The experimental data exhibit a fission decline at high neutron multiplicity which is not reproduced by the model combining INC with GEMINI. A much better agreement is found when plugging PACE after
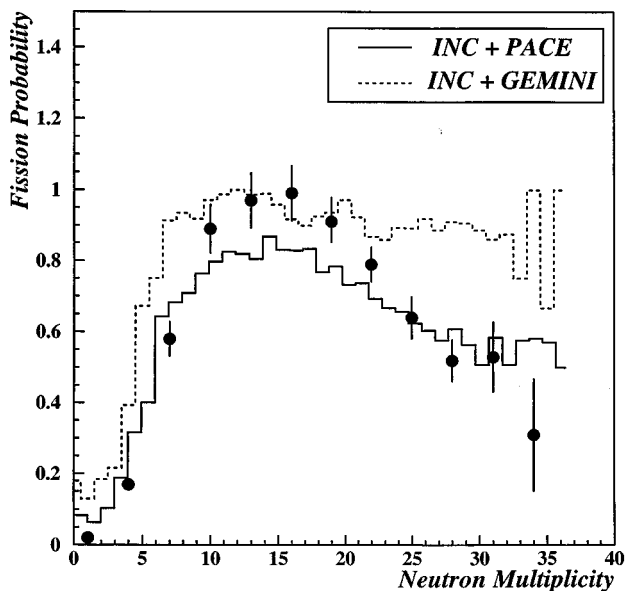
FIG. 20. Same as Fig. 19, for 2 GeV ^{3}He+U.
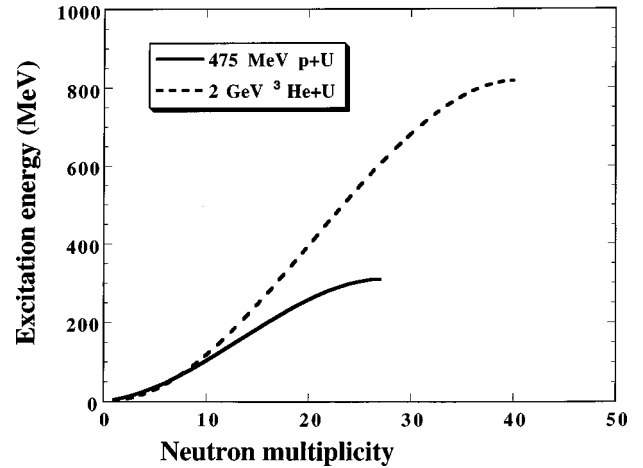
FIG. 21. Computed excitation energies at the end of the INC step as a function of neutron multiplicity (the latter is folded with detection efficiency) for 475 MeV p+U and 2 GeV ^{3}He+U.

the INC, instead of GEMINI. The maximum fission probability is observed for the same neutron multiplicity in experimental and modeled data. The 15% difference in the absolute probability is within the experimental uncertainty of the absolute normalization between inclusive and exclusive experimental data. It should be noted that an agreement close to the one shown for PACE was also obtained by Hilscher [68], taking a similar approach using JULIAN. Why are GEMINI and PACE, both using the transition state model, deviating in their prediction of the fission probabilities? The inclusion of IMF emission in GEMINI, treated as a very asymmetric scission configuration, should hinder a subsequent standard fission rather than favor it. Hence, the too low IMF emission given by GEMINI could be taken as responsible for the too high fission probability predicted by GEMINI.

The differences in measured fission probabilities between the two systems for a given neutron multiplicity may appear surprising. As a matter of fact this can be due to the different populations of nuclei after the INC. It is shown in Fig. 21 that the events registered with the same M_n correspond, on the average, to hotter nuclei in ^{3}He-induced reactions than in proton reactions.

A detailed account of the model calculations for fission is given in Fig. 22 for the 2 GeV ^{3}He+U system. In the upper panel the population of nuclei as a function of their atomic number Z and mass A is shown at the end of the INC step (taken at 30 fm/c). The mean excitation energy for the thus formed nuclei is given in the middle panel, clearly indicating that the products with the largest mass deficit are among the hottest ones, as expected when a large number of nucleons have been involved in the INC process. Finally, in the bottom panel, the fission probability of the nuclei is given, as computed with PACE. The effects of nuclear fissility (function of Z^2/A) and excitation energy are well exhibited with both the high-Z nuclei and neutron-poor nuclei showing the largest chance to undergo fission. The used experimental setup did not allow these predictions to be checked in such detail but it allows nevertheless understanding the rise and fall of the fission probability with excitation energy (neutron number) as shown in Fig. 20. On the one hand, at low excitation energy (low measured neutron multiplicity) nuclei not
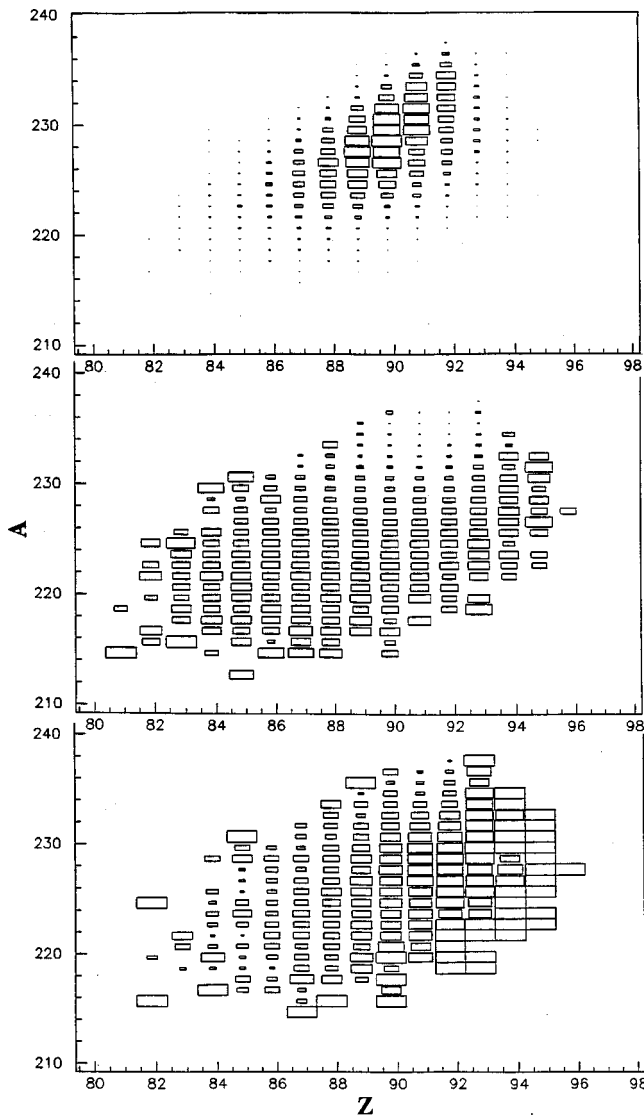
FIG. 22. Top panel: population of nuclei after the INC step for 2 GeV ^{3}He+U, as a function of Z and A. Middle panel: excitation energy. Bottom panel: fission probability. The size of the boxes is proportional to the considered quantities.

having undergone fission are to be found as rather heavy residues. On the other hand, at high excitation energy (large measured neutron multiplicity), the nuclei having escaped fission must be found very light: indeed they must have suffered first a long INC step in order to built up excitation energy and then a long evaporation chain in order to cool down. Because of their low final masses, such residues might be confused with fission fragments and only coincidence experiments using 4π detectors such as those of Ref. [18] can allow a detailed study of the decay process.

It is worth noticing that the present fission data at high excitation energy are consistent with those obtained in antiproton-induced reactions at 1.2 GeV on U, with a fission probability of about 30% at $E^*=750$ MeV [69].

VI. SUMMARY AND PROSPECTS

The purpose of the present experiment was to investigate the conditions of formation and decay of nuclei heated by light projectiles which avoid the inherent complications of heavy-ion reactions. In particular, using light projectiles, the buildup of collective excitation (rotational, compressional, deformation) is strongly reduced. The experiment was performed using the neutron multiplicity as the key observable for the heat deposited in the nucleus. This observable is shown to be most representative since it remains meaningful for all degrees of energy dissipation and thus allows one to probe essentially the total reaction cross section. All experimental data were compared with those generated in a two-step model including a preequilibrium stage based on an intranuclear cascade (INC from Cugnon [22]), followed by a sequential decay from a thermally equilibrated system, including light particle evaporation (neutrons and various isotopes of H and He), IMF emission, and fission, using the GEMINI [45] computer code. All available observables were compared to the model calculations in a very consistent and constraining way, since for the first time in such reaction studies there are many distinct observables linked together through the neutron multiplicity. The measured neutron multiplicities, taking into account the efficiency of the neutron detector, were shown to be fairly well reproduced by the two-step model. Choosing an average thermalization time of 30 fm/c, an excitation energy spectrum could be inferred from the model, showing that Au-like nuclei were excited to energies of more than 500 MeV in approximately 10% of all events. This result proves that high temperatures can be reached in light-particle-induced collisions.

Then the evaporation of light charged particles and IMF was considered as a function of neutron multiplicity. It was shown that, at any angle, the emission of clustered particles with $Z=2$ or 3 is never fully evaporative whatever the type of projectile—proton or ^{3}He—and whatever the initial collision: peripheral with low deposited energy or, on the contrary, central and thus more dissipative. The energy spectra show a deviation from a purely evaporative behavior at all angles with the strength of highly energetic particles growing from backward to forward angles. The INC models are unable to account for this effect and this poses a challenge to theory to reproduce it. The preequilibrium emission of these clusters may have consequences on the rest of the data which are still difficult to foresee. As for the evaporative yield, it is rather well reproduced at least for $Z=1,2$ particles together with the associated neutrons. The emission of evaporative IMF's (mostly Li, Be, and B) is underestimated by the model, but their multiplicity is smaller than in nucleus-nucleus collisions, thus clearly showing that the dynamics and the collective excitations are responsible for the high multiplicities measured in nucleus-nucleus collisions.

Finally, fission has been investigated as a function of neutron multiplicity. A smooth evolution in the velocity distribution of the fissioning nucleus was observed as well as broadening effects with increasing energy dissipation. Although a similar trend was observed in the two-step model for events ending by fission of the hot targetlike nuclei, the absolute values of the folding angle of the fission fragments could not be reproduced. The reasons for this disagreement are not yet clear. Similarly, although the fission probability was satisfactorily reproduced for the 475 MeV proton experiment at all excitation energies, a disagreement was observed for the ^{3}He experiment at high excitation energies. The

GEMINI model overpredicts the fission probability increasingly as the thermal energy increases. A better agreement is obtained using PACE instead of GEMINI. The process taking over from fission at high excitation energy could be the generation of evaporation residues or the so-called multifragmentation process, i.e., a simultaneous breakup of the excited nucleus into more than two fragments [70–73]. Considering the rather low multiplicity of IMF's measured at high excitation energies (0.25 evaporationlike IMF per event) and their nature (mostly Li and to a lesser extent Be, B, etc.), it is very doubtful that multifragmentation is responsible for the drop of fission. As predicted by PACE, evaporation residue formation appears to be the most likely alternative to binary fission. However, because of their low recoil velocity, it is hopeless to get the heavy residues out of the target and measure them in flight without loss. Only the detection of their characteristic γ rays or K x rays may provide a handle on them. As for thermally driven multifragmentation at these bombarding energies with proton projectiles, it is planned to use in the near future a 4π charged particle detector in coincidence with a 4π neutron detector in order to establish or disprove its existence. As was stressed by Hüfner in a review article [74] ten years ago, it is only in very exclusive experiments that progress could really be made in the understanding of proton-nucleus reactions.

The present type of study is receiving a renewed interest in conjunction with intense neutron spallation sources for various applications, be it for neutron scattering [75], transmutation of nuclear wastes [76], or energy amplifiers [77]. Much progress has been made recently in spallation neutron production studies on thin as well as thick targets [78–80].

[1] J. N. De, N. Rudra, Subrata Pal, and S. K. Samaddar, Phys. Rev. C **53**, 780 (1996).

[2] M. Brack and P. Quentin, Phys. Scr. **T10**, 163 (1974).

[3] M. Brack and P. Quentin, Phys. Lett. **52B**, 159 (1974).

[4] P. Bonche, S. Levit, and D. Vautherin, Nucl. Phys. **A427**, 278 (1984).

[5] P. Bonche, S. Levit, and D. Vautherin, Nucl. Phys. **A436**, 265 (1985).

[6] S. Levit and P. Bonche, Nucl. Phys. **A437**, 426 (1985).

[7] D. R. Dean and U. Mosel, Z. Phys. A **322**, 647 (1985).

[8] E. Suraud, Nucl. Phys. **A462**, 109 (1987).

[9] H. Q. Song and R. K. Su, Phys. Rev. C **44**, 2505 (1991).

[10] M. Baldo, Y. H. Cai, G. Giansiracusa, U. Lombardo, and H. Q. Song, Phys. Lett. B **340**, 13 (1994).

[11] J. Nemeth, M. Barranco, C. Ngô, and E. Tomasi, Z. Phys. A **323**, 419 (1986).

[12] D. Vautherin, J. Treiner, and M. Vénéroni, Phys. Lett. B **191**, 6 (1987).

[13] J. Galin, B. Gatty, D. Guerreau, C. Rousset, U. C. Schlotthauer-Voos, and X. Tarrago, Phys. Rev. C **9**, 1113 (1974).

[14] J. Galin, B. Gatty, D. Guerreau, C. Rousset, U. C. Schlotthauer-Voos, and X. Tarrago, Phys. Rev. C **9**, 1126 (1974).

[15] T. Ethvignot, A. Elmaani, N. N. Ajitanand, J. M. Alexander, E. Bauge, P. Bier, L. Kowalski, M. T. Magda, P. Désesquelles, H. Elhage, A. Giorni, D. Heuer, S. Kox, A. Lleres, F. Merchez, C. Morand, D. Rebreyend, P. Stassi, J. B. Viano, S. Benrachi, B. Chambon, B. Cheynis, D. Drain, and C. Pastor, Phys. Rev. C **43**, 2035 (1991).

[16] B. Jouault, V. de la Mota, F. Sébille, G. Royer, and J. F. Lecolley, Nucl. Phys. **A597**, 136 (1996).

[17] L. Pienkowski, H. G. Bohlen, J. Cugnon, H. Fuchs, J. Galin, B. Gatty, B. Gebauer, D. Guerreau, D. Hilscher, D. Jacquet, U. Jahnke, M. Josset, X. Ledoux, S. Leray, B. Lott, M. Morjean, A. Péghaire, G. Röschert, H. Rossner, R. H. Siemssen, and C. Stéphan, Phys. Lett. B **336**, 147 (1994).

[18] F. Goldenbaum, W. Bohne, J. Eades, T. von Egidy, P. Figuera, H. Fuchs, J. Galin, Ye. S. Golubeva, K. Gulda, F. J. Hartmann, D. Hilscher, A. S. Iljinov, U. Jahnke, J. Jastrzebski, W. Kurcewicz, B. Lott, M. Morjean, G. Pausch, A. Péghaire, L. Pienkowski, D. Polster, S. Proschitzki, B. Quednau, H. Rossner, S. Schmid, W. Schmid, and P. Ziem, Phys. Rev. Lett. **77**, 1230 (1996).

[19] W. G. Meyer, H. H. Gutbrod, Ch. Lukner, and A. Sandoval, Phys. Rev. C **22**, 179 (1979).

[20] K. B. Morley, K. Kwiatkowski, D. S. Bracken, E. Renshaw Foxford, V. E. Viola, L. W. Woo, N. R. Yoder, R. Legrain, E. C. Pollacco, C. Volant, R. G. Korteling, H. Breuer, and J. Brzychczyk, Phys. Rev. C **54**, 737 (1996).

[21] E. Renshaw Foxford, K. Kwiatkowski, D. S. Bracken, K. B. Morley, V. E. Viola, N. R. Yoder, C. Volant, E. C. Pollacco, R. Legrain, R. G. Korteling, W. A. Friedman, J. Brzychczyk, and E. Breuer, Phys. Rev. C **54**, 749 (1996).

[22] J. Cugnon, Nucl. Phys. **A462**, 751 (1987).

[23] J. Cugnon, P. Jasselette, and J. Vandermeulen, Nucl. Phys. **A470**, 558 (1987).

[24] J. Cugnon and J. Vandermeulen, Ann. Phys. (Paris) **14**, 49 (1989).

[25] A. S. Botvina, A. S. Iljinov, and I. N. Mishustin, Phys. Lett. B **205**, 421 (1988).

[26] Ye. S. Golubeva, A. S. Iljinov, A. Botvina, and N. M. Sobolevsky, Nucl. Phys. **A483**, 539 (1988).

[27] H. Delagrange, C. Grégoire, F. Scheuter, Y. Abe, Z. Phys. A **323**, 437 (1986).

[28] G. F. Bertsch, Z. Phys. A **289**, 103 (1978).

[29] D. Brink, Nucl. Phys. **A519**, 3c (1990).

[30] K. Niita, S. Chiba, T. Maruyama, T. Maruyama, H. Takada, T.

Fukahori, Y. Nakahara, and A. Iwamoto, Phys. Rev. C **52**, 2620 (1995).

[31] B. E. Bonner, J. E. Simmons, C. R. Newsom, P. J. Riley, D. Glass, J. C. Hiebert, Mahavir Jain, and L. C. Northcliffe, Phys. Rev. C **18**, 1418 (1978).

[32] J. W. Wachter, W. A. Gibson, and W. R. Burrus, Phys. Rev. C **6**, 1496 (1972).

[33] D. B. Barlow, B. M. K. Nefkens, C. Pillai, J. W. Price, I. Slaus, M. J. Wang, J. A. Wightman, K. W. Jones, M. J. Leitch, C. S. Mishra, C. L. Morris, J. C. Peng, P. K. Peng, and J. M. Tinsley, Phys. Rev. C **45**, 293 (1992).

[34] S. Cierjacks, Y. Hino, F. Raupp, L. Buth, D. Filges, P. Cloth, and T. W. Armstrong, Phys. Rev. C **36**, 1976 (1987).

[35] E. K. Hyde, G. W. Butler, and A. M. Poskanzer, Phys. Rev. C **4**, 1759 (1971).

[36] A. M. Poskanzer, R. G. Sextro, A. M. Zebelman, H. H. Gutbrod, A. Sandoval, and R. Stock, Phys. Rev. Lett. **35**, 1701 (1975).

[37] S. J. Yennello, K. Kwiatkowski, D. E. Fields, R. Planeta, V. E. Viola, E. C. Pollacco, C. Volant, R. Dayras, R. Legrain, Y. Cassagnou, S. Harar, and E. Hourani, Phys. Lett. B **246**, 26 (1990).

[38] K. Nakai, T. A. Shibata, H. Enmyo, S. Sasaki, M. Sekimoto, I. Arai, K. Nakayama, K. Ichimaru, H. Nakamura-Yokota, and R. Chiba, Phys. Lett. **121B**, 373 (1983).

[39] B. Lott, J. L. Charvet, E. Crema, G. Duchêne, H. Doubre, J. Fréhaut, J. Galin, B. Gatty, D. Guerreau, G. Ingold, D. Jacquet, U. Jahnke, D. X. Jiang, C. Magnago, M. Morjean, Y. Patin, E. Piasecki, J. Pouthas, Y. Pranal, F. Saint-Laurent, E. Schwinn, A. Sokolov, J. L. Uzureau, and X. M. Wang, Z. Phys. A **346**, 201 (1993).

[40] J. Galin and U. Jahnke, J. Phys. G **20**, 1105 (1994).

[41] Y. Périer, B. Lott, Y. El-Masri, J. Galin, Th. Keutgen, M. Morjean, A. Péghaire, B. M. Quednau, and I. Tilquin, Nucl. Instrum. Methods Phys. Res. A (to be published).

[42] M. Wilpert, B. Gebauer, Th. Wilpert, W. von Oertzen, H. G. Bohlen, and J. Speer, Phys. Rev. C **51**, 680 (1995).

[43] U. Jahnke, G. Ingold, D. Hilscher, H. Orf, E. A. Koop, G. Feige, and R. Brandt, *Lecture Notes in Physics* (Springer-Verlag, Berlin, 1983), Vol. 178, p. 179.

[44] P. U. Renberg, D. F. Measday, M. Pepin, P. Schwaller, B. Favier, and C. Richard-Serre, Nucl. Phys. **A183**, 81 (1972), and references therein.

[45] GEMINI, a computer code developed by R. J. Charity; see R. J. Charity, M. A. McMahan, G. J. Wozniak, R. J. McDonald, L. G. Moretto, D. G. Sarantites, L. G. Sobotka, G. Guarino, A. Pantaleo, L. Fiore, A. Gobbi, and K. Hildenbrand, Nucl. Phys. **A483**, 371 (1988).

[46] PACE, a computer code developed by A. Gavron, Phys. Rev. C **21**, 230 (1980).

[47] DENIS, a computer code developed by J. Poitou and C. Signarbieux, Nucl. Instrum. Methods **114**, 113 (1974).

[48] GEANT, a computer code developed at CERN by R. Brun *et al.*, CERN Report DD/EE/82, 1982.

[49] A. Y. Abul-Magd, W. A. Friedman, and J. Hüfner, Phys. Rev. C **34**, 113 (1986).

[50] M. Morjean, C. Lebrun, D. Ardouin, A. Chbihi, H. Dabrowski, B. Erazmus, P. Eudes, J. Galin, D. Guerreau, F. Guilbault, C. Ghisalberti, D. Jacquet, P. Lautridou, R. Lednicki, A. Péghaire, Y. Périer, J. Pluta, J. Quebert, A. Rahmani, T.

Reposeur, L. Sezac, and R. H. Siemssen, Nucl. Phys. **A591**, 371 (1995).

[51] G. Peilert, J. Konopka, H. Stöcker, W. Greiner, M. Blann, and M. G. Mustafa, Phys. Rev. C **46**, 1457 (1992).

[52] J. Aichelin (private communication).

[53] R. E. L. Green, K. G. Korteling, J. M. D'Auria, K. P. Jackson, and R. L. Helmer, Phys. Rev. C **35**, 1341 (1987).

[54] R. E. L. Green and R. G. Korteling, Phys. Rev. C **22**, 1594 (1980).

[55] R. T. de Souza, L. Phair, D. R. Bowman, N. Carlin, C. K. Gelbke, W. G. Gong, Y. D. Kim, M. A. Lisa, W. G. Lynch, G. F. Peaslee, M. B. Tsang, H. M. Xu, and F. Zhu, Phys. Lett. B **268**, 6 (1991).

[56] A. Sokolov, D. Guerreau, J. L. Charvet, B. Cramer, H. Doubre, J. Fréhaut, J. Galin, B. Gatty, G. Ingold, D. Jacquet, U. Jahnke, D. X. Jiang, B. Lott, C. Magnago, M. Morjean, Y. Patin, E. Piasecki, J. Pouthas, and E. Schwinn, Nucl. Phys. **A562**, 273 (1993).

[57] J. F. Lecolley, L. Stuggé, M. Aboufirassi, B. Bilwes, R. Bougault, R. Brou, F. Cosmo, J. Colin, D. Durand, J. Galin, A. Genoux-Lubain, D. Guerreau, D. Horn, D. Jacquet, J. L. Laville, F. Lefebvres, C. Le Brun, O. Lopez, M. Louvel, M. Mahi, C. Meslin, M. Morjean, A. Péghaire, G. Rudolf, F. Scheibling, J. C. Steckmeyer, B. Tamain, and S. Tomasevic, Phys. Lett. B **354**, 202 (1995).

[58] J. Tõke, B. Lott, S. P. Baldwin, B. M. Quednau, W. U. Schröder, L. G. Sobotka, J. Barreto, R. J. Charity, D. G. Sarantites, D. W. Stracener, and R. T. de Souza, Phys. Rev. Lett. **75**, 2920 (1995).

[59] L. P. Remsberg, F. Plasil, J. B. Cumming, and M. L. Perlman, Phys. Rev. C **1**, 265 (1970).

[60] L. P. Remsberg, F. Plasil, J. B. Cumming, and M. L. Perlman, Phys. Rev. **187**, 1597 (1969).

[61] J. Galin, M. Lefort, J. Péter, X. Tarrago, E. Cheifetz, and Z. Frankel, Nucl. Phys. **A134**, 513 (1969).

[62] B. D. Wilkins, S. B. Kaufman, E. P. Steinberg, J. A. Urbon, and D. J. Henderson, Phys. Rev. Lett. **43**, 1080 (1979).

[63] F. Saint-Laurent, M. Conjeaud, R. Dayras, S. Harar, H. Oeschler, and C. Volant, Phys. Lett. **110B**, 372 (1982).

[64] L. N. Andronenko, A. A. Kotov, M. M. Nesterov, V. F. Petrov, N. A. Tarasov, L. A. Vaishnene, and W. Neubert, Z. Phys. A **138**, 97 (1984).

[65] Z. Fraenkel, A. Breskin, R. Chechik, S. Wald, R. Abegg, H. W. Fielding, P. Kitching, S. T. Lam, G. C. Neilson, W. C. Olsen, and J. Uegaki, Phys. Rev. C **41**, 1050 (1990).

[66] G. Klotz-Engmann, H. Oeschler, J. Stroth, E. Kankeleit, Y. Cassagnou, M. Conjeaud, R. Dayras, R. Legrain, E. C. Pollacco, and C. Volant, Nucl. Phys. **A499**, 392 (1989).

[67] M. H. Simbel, Z. Phys. A **333**, 177 (1989).

[68] D. Hilscher, in *Proceedings of the XV Nuclear Physics Conference on Low Energy Nuclear Dynamics, Saint-Petersburg, 1995*, edited by Yu. Oganessian, W. von Oertzen, and R. Kalpakchieva (World Scientific, Singapore, 1995), p. 169.

[69] F. Goldenbaum, Ph.D. thesis, Freie Universität Berlin, 1997 (unpublished).

[70] D. H. E. Gross, Rep. Prog. Phys. **53**, 605 (1990).

[71] J. P. Bondorf, R. Donangelo, I. N. Mishustin, C. J. Pethick, H. Schulz, and K. Sneppen, Nucl. Phys. **A443**, 321 (1985).

[72] J. P. Bondorf, R. Donangelo, I. N. Mishustin, and H. Shulz, Nucl. Phys. **A444**, 460 (1985).

[73] H. W. Barz, J. P. Bondorf, R. Donangelo, I. N. Mishustin, and

H. Shulz, Nucl. Phys. **A448**, 753 (1986).

[74] J. Hüfner, Phys. Rep. **125**, 130 (1985).

[75] I. S. K. Gardener, H. Lengeler, and G. H. Rees, report on the European Spallation Source, ESS 95-30-M, 1995.

[76] C. D. Bowman, E. D. Arthur, P. W. Lisowski, G. P. Lawrence, R. J. Jensen, J. L. Anderson, B. Blind, M. Cappiello, J. W. Davidson, T. R. England, L. N. Engel, R. C. Haight, H. G. Hughes III, J. R. Ireland, R. A. Krakowski, R. J. LaBauve, B. C. Letellier, R. T. Perry, G. J. Russel, K. P. Staudhammer, G. Versanis, and W. B. Wilson, Nucl. Instrum. Methods Phys. Res. A **320**, 336 (1992).

[77] S. Andriamonge *et al.*, Phys. Lett. B **348**, 697 (1995).

[78] D. Hilscher, F. Goldenbaum, U. Jahnke, L. Pienkowski, J. Galin, B. Lott, and B. Quednau, *Workshop on Nuclear Methods for Transmutation of Nuclear Waste*, 1996, Dubna, Russia, edited by M. Kh. Khankhasayev, H. S. Plendl, and Z. B. Kurmanov (World Scientific, Singapore, 1997), p. 176.

[79] L. Pienkowski, F. Goldenbaum, D. Hilscher, U. Jahnke, J. Galin, and B. Lott, Phys. Rev. C **56**, 1909 (1997).

[80] D. Hilscher, U. Jahnke, F. Goldenbaum, L. Pienkowski, J. Galin, and B. Lott, Nucl. Instrum. Methods Phys. Res. A (to be published).